IET Microwaves, Antennas & Propagation

Research Article

IET Journals
The Institution of Engineering and Technology

Ultra wideband compact near-field imaging system for breast cancer detection

ISSN 1751-8725
Received on 10th June 2014
Revised on 4th February 2015
Accepted on 4th February 2015
doi: 10.1049/iet-map.2014.0735
www.ietdl.org

Malyhe Jalilvand ✉, *Xuyang Li, Lukasz Zwirello, Thomas Zwick*

Institut für Hochfrequenztechnik und Elektronik, IHE, Karlsruhe Institute of Technology, KIT, Karlsruhe, Germany
✉ *E-mail: malyhe.jalilvand@kit.edu*

Abstract: In this study, an efficient near-field imaging system using miniaturised bowtie antennas is proposed for the three-dimensional (3D) detection of breast tumours. To ensure good penetration and high resolution, a novel compact bowtie antenna is developed. The antenna features a high fractional bandwidth covering both low and high frequencies, while still small in size. A hemispherical array of 16 compact bowtie antennas is built and following a multistatic scenario, scattered signals from two breast phantoms with one and two embedded tumours inside are recorded. The radar-based set-up operates in the frequency range of 1.2–7 GHz. It is shown that the imaging system can successfully detect the tumour phantoms in 3D space.

1 Introduction

During the last decade, microwave-based medical imaging systems and especially ultra wideband (UWB) imaging have been widely exploited and investigated both as a complementary method to the available imaging techniques and as an alternative solution. Contrary to X-rays, microwaves are non-ionising and therefore allow frequent examinations. Furthermore, this technology is compact and relatively cheap in comparison with conventional medical imaging techniques such as magnetic resonance imaging [1, 2].

For years, there has been a lot of research aiming at early breast cancer detection [3–8], but recently the research has been extended to bone imaging [9] and stroke detection in human head as well [10]. For the diagnosis of breast cancer, X-ray mammography is so far the main imaging modality. However, in addition to a rather high false-alarm rate, the technique suffers from major drawbacks such as ionising radiation and an uncomfortable procedure [11].

The aforementioned limitations of the conventional techniques have motivated the research for alternative imaging modalities among which microwave imaging has raised a great interest. Microwave imaging is based on the contrast of the dielectric properties of healthy tissues and abnormalities. In the case of breast cancer, the dielectric properties of tumour are known to be higher than those of the normal breast (and fibro glandular parenchyma) leading to a contrast, which is necessary for the successful application of microwave approach [12]. The reported clinical results are encouraging and prove the high potential of microwave techniques [13, 14].

Another interesting approach in recent years has been that of hybrid imaging modalities [15–18]. For instance, an interesting complementary imaging technique suggested for breast cancer detection is microwave-induced thermoacoustic imaging that combines the high contrast of microwave with the high resolution of ultrasound [16].

The general microwave imaging approach consists of illuminating the target with microwave signals and recording the scattered signals in different directions. Owing to the contrast of the dielectric properties of the biological layers, the recorded signals can provide important information about the target. Using an efficient processing of the recorded signals, it is possible to obtain the relative energy map (in confocal radar approach [3–6]) or the dielectric map (in microwave tomography [19, 20]) of the target.

The final goal of microwave imaging technology is the development of a low-cost and reliable imaging system that can be easily adopted to clinical situations. Antennas play an important role in realising successful and efficient imaging systems. For the successful operation of radar-based imaging systems that are based on illuminating the target with UWB signals, the antenna under the test should fulfil the following requirements:

(1) efficient direction of power into the breast,
(2) compact nature for enabling integration of large number of elements in the antenna array,
(3) ability to transmit and receive signals in a broad frequency range, including both low and high frequencies, in order to guarantee high resolution as well as good penetration into biological tissues,

Most of the antennas designed so far for early breast cancer detection (e.g. [13, 21–25]), cover the spectrum of nearly 4–10 GHz, which corresponds to a fractional bandwidth of 85%. However, to ensure sufficient penetration into the breast tissue (especially into the low-adipose tissues [12]), radiations at lower frequencies around 1 GHz are favourable. Since the dimension of the antenna is wavelength dependent, the design of a compact antenna that covers lower frequencies is quite a challenge.

In this paper, the idea behind the antenna design is same as the one presented by Jalilvand *et al.* [26]; that is, addition of inductive strips to compensate the capacitive nature of the antenna. However, in this work, the antenna was further optimised for application in UWB breast cancer detection. The final goal was to design a compact element capable of efficiently transceiving signals in UWB spectrum including reasonably low frequencies. The novel compact structure can efficiently radiate electromagnetic waves starting from 1.2 GHz. The antenna performance was evaluated via both simulations and measurements. Later, the proposed antenna was implemented inside a hemispherical array as a part of an UWB near-field imaging system for breast cancer detection.

The organisation of the paper is as follows. In Section 2 the near-field imaging system is introduced; it includes the characterisation of the antenna, the explanation of the measurement set-up and the breast mimicking phantoms. Results are discussed in Section 3 and finally the paper ends up with conclusion in Section 4.

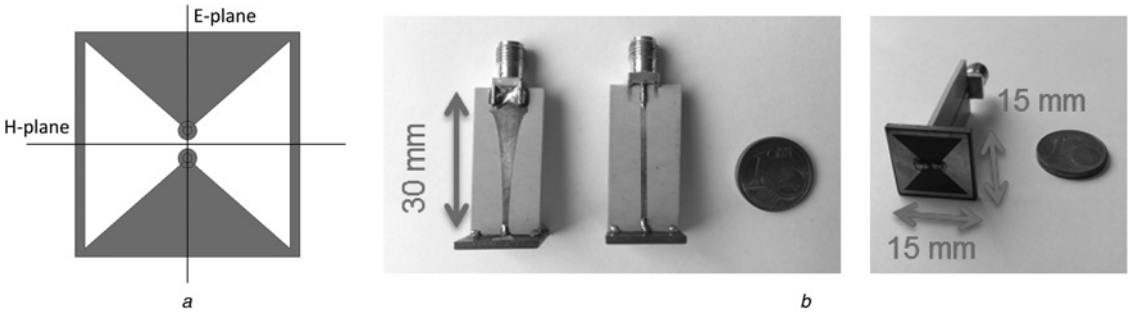

Fig. 1 *Modified bowtie antenna with the inductive strips and the balun feeding*

a Schematic diagram of the antenna
b Different views of the manufactured antenna

2 Near-field imaging system

2.1 Miniaturised UWB antenna

In confocal radar imaging, it is desired to have a compact UWB antenna element that will efficiently transmit and receive signals with a minimal level of dispersion. Broadband bowtie antenna with its stable phase centre is a very appealing choice for this approach. The antenna presented in this work is a modified version of the bowtie antenna presented in [27] for medical imaging. With the two arms of the conventional bowtie antenna being short-connected (see Fig. 1*a*), the capacitive nature of the antenna is partly compensated and therefore, it is possible to optimise the dimension of the antenna so that it will radiate efficiently in a broadband spectrum. The balun transition of the feeding structure also leads to a symmetrical radiation in the bandwidth of interest.

Previously, an antenna design was presented by Jalilvand *et al.* [26] in which the element was meant to be used in microwave tomography-based imaging systems for the detection of stroke in human head. For breast cancer detection using UWB radar, the antenna in [26] has been further optimised to cover a wide frequency range starting from around 1 GHz to ensure good penetration into the breast. The structure of the new antenna can be seen in Fig. 1. The radiating part of the antenna has the dimension of 15 mm which is quite compact. The feeding network and the bowtie were constructed on different substrates; Rogers 6110 with a relative permittivity of 10.2 and thickness of 1.27 mm was used for the feeding and to ensure reasonable dimensions of the feeding network in comparison to the bowtie (Rogers 5880 with relative permittivity of 2.2 and thickness of 1.57 mm was used for the radiating bowtie).

The antenna was specially optimised for early breast cancer detection, therefore the bowtie was either in direct contact to a breast-mimicking phantom or inside a matching liquid representing an average relative permittivity of $\varepsilon = 20$. The feeding balun must be, however, inside a low-permittivity environment to ensure the directional radiation of the antenna into the phantom or matching liquid. The reflectivity of the designed antenna was measured with the bowtie inside a polyethylene glycol (PEG)–water solution having a relative permittivity of 18 at 4 GHz, while the feeding network was kept in air. In Fig. 2, the simulated and measured reflection coefficients of the antenna are displayed. It was observed both in simulation and measurement that the reflectivity of the antenna stays below −8 dB in the bandwidth of 1.2 – 7 GHz.

The simulated electric field of the antenna is displayed in Fig. 3. As observed in the figure, the electric field began to radiate into two separate directions starting from 7 GHz (Fig. 3*d*). Since in near-field imaging we are interested in directional antennas, in this case the frequencies higher than 7 GHz were not practical. Therefore the compact bowtie antenna having a maximum

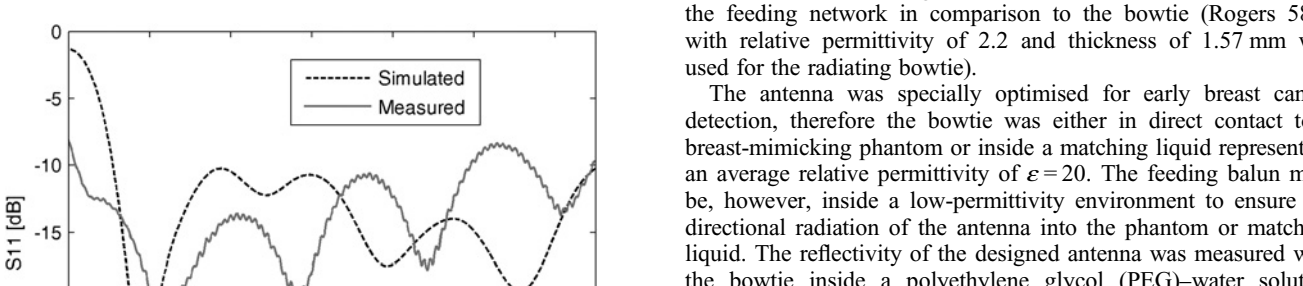

Fig. 2 *Simulated and measured reflection coefficient of the bowtie antenna in the PEG solution*

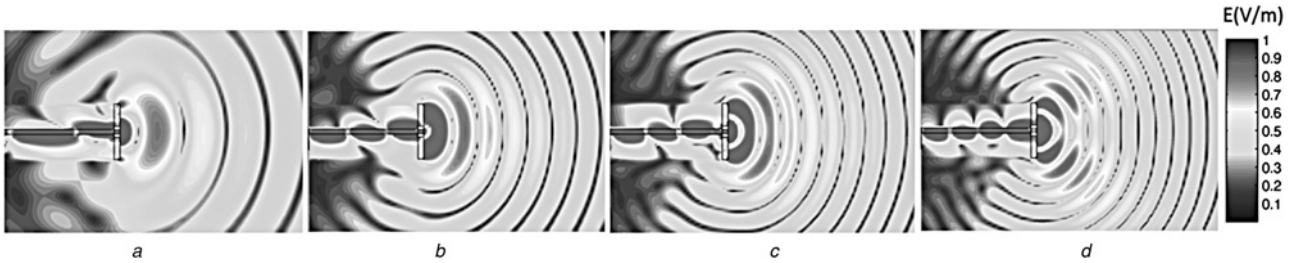

Fig. 3 *Simulated normalised electric field distribution of the antenna (in the near-field region) with the background permittivity of 20 at*

a 4 GHz
b 5 GHz
c 6 GHz
d 7 GHz

IET Microw. Antennas Propag., 2015, Vol. 9, Iss. 10, pp. 1009–1014

dimension of 15 mm × 15 mm and a bandwidth of 1.2 – 7 GHz (corresponding to a fractional bandwidth of 141.46%) was later used in our near-field imaging system for detection of tumour in synthesised breast phantoms.

2.2 UWB imaging system

In this section, the near-field imaging system including the measurement set-up for collecting the scattered signals and the breast phantoms are reviewed.

2.2.1 Measurement set-up: To realise a realistic set-up having the potential of being later employed in clinical trials, a 16-element hemispherical array was implemented. As explained in the previous section, the bowtie antennas were designed to work between two media; that is, the radiating bowtie was in contact to a breast-mimicking phantom, whereas the feeding network was kept inside a low-permittivity medium (preferably air). With that in mind, for the laboratory set-up, a polystyrene hemisphere was chosen as the base of the array. The dielectric properties of polystyrene were very close to those of air, making it a good medium for the background in the initial laboratory implementation. The hemisphere had an inner radius of 5.45 cm.

To arrange 16 antennas on a hemispherical surface, two important criteria were considered: the antenna elements were positioned so that the adjacent elements were as equi-distant as possible. Moreover, as it was discussed in [28], to have a good cross-range resolution, it was preferred to arrange the antenna elements in a rectangular form. Having considered these two criteria, the final arrangement of the array displayed in Fig. 4 was chosen.

The E8363B vector network analyser (VNA) from Agilent Technologies was used as the radio-frequency (RF) transmitter and receiver. The output power of VNA was 5 dBm, the intermediate frequency bandwidth was set to 300 Hz and 1601 points were considered in the bandwidth from 1 to 7.5 GHz. Furthermore, a power amplifier of ∼11 dB gain was connected to the VNA output leading to a final output power of around 16 dBm. For the collection of signals, a multistatic scenario was adopted and the antenna elements of the array acted sequentially as transmitter, whereas all the other antennas acted as receiver (Rx). A programmed RF mechanical switch matrix was used to automatically connect each Tx–Rx antenna pair to the VNA, resulting in 240 different measurements, half of which were considered for the imaging because of the reciprocity. A sketch of the near-field imaging system together with a picture of the implemented imaging system is shown in Fig. 5.

2.2.2 Breast phantom: For the evaluation of the proposed near-field imaging system, a hemispherical breast phantom of radius 5.45 cm was built. The breast phantom was a mixture of water (47%), sugar (47%) and gelatin (6%). The tumour phantom

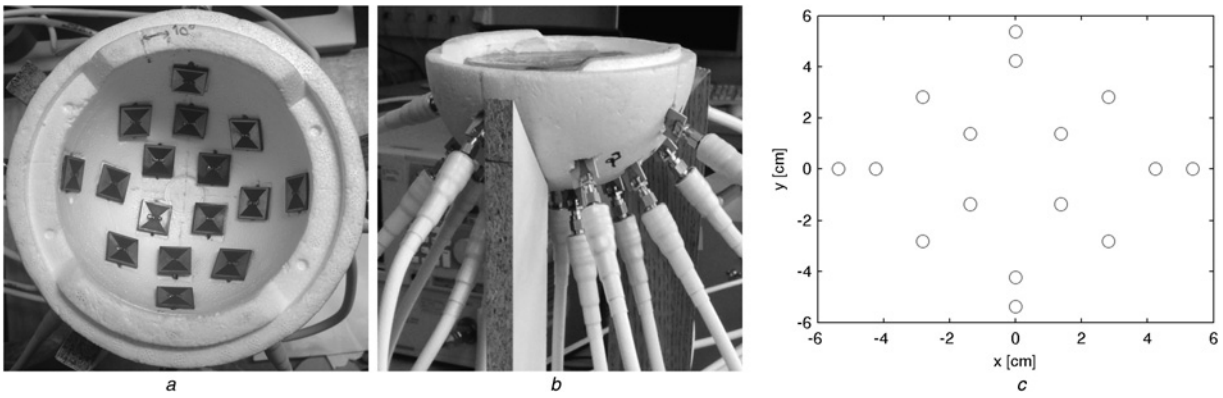

Fig. 4 *Final arrangement of the array*

a, b Array configuration on a styropor base
c Two-dimensional mapped positions of the antenna elements

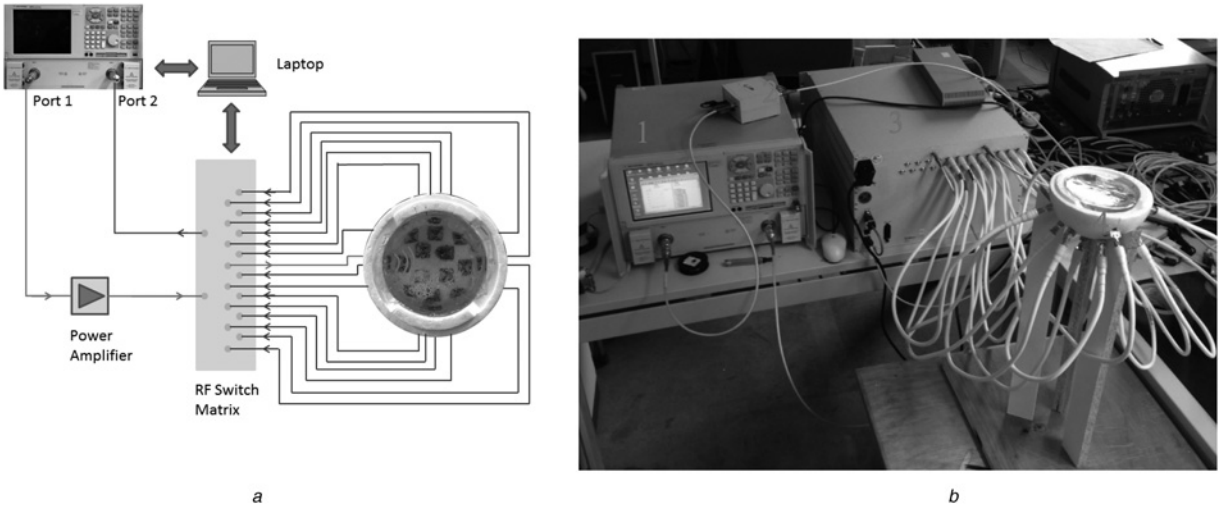

Fig. 5 *Sketch of the near-field imaging system and a picture of the implemented imaging system*

a Schematic diagram of the imaging system
b Actual implemented near-field imaging system
1 – VNA, 2 – power amplifier, 3 – mechanical switch matrix and 4 – antenna array with breast phantom inside

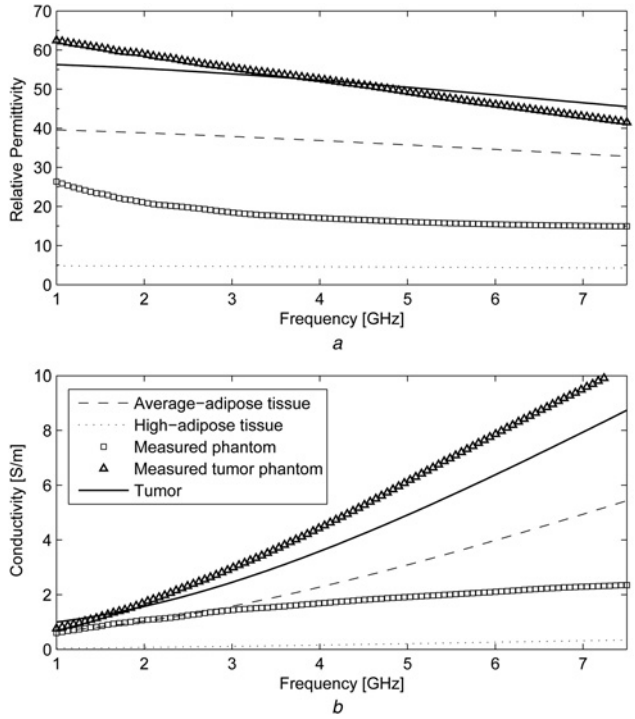

Fig. 6 *Relative permittivity and conductivity of normal breast tissue and tumour as obtained from the Cole–Cole equation [29] compared with the measured dielectric properties of the synthesised breast phantom*

a Relative permittivity
b Conductivity

was ~10 mm in diameter and was made up of the same ingredients, however, with the following proportions: water (71%), sugar (14.5%) and gelatin (14.5%).

The permittivity and conductivity of the breast phantom and tumour were measured using the Agilent Dielectric Probe Kit (85070E) and were compared with the corresponding values predicted by Cole–Cole formula [12] in Fig. 6. As shown in the figure, the measured values for the breast phantom were between the high and average adipose categories of normal breast. The synthesised phantoms with one and two tumours are displayed in Fig. 7.

3 Results and discussion

As explained previously, using UWB antenna array consisting of 16 elements (Fig. 4) and the breast phantoms shown in Fig. 7, 120 signals in frequency range of $1.2 - 7$ GHz were recorded. For data calibration, since we were only interested in the response of the tumour, a second measurement was performed with the array being 15° rotated and the resultant signals were subtracted correspondingly [30]. This allows for removal of unwanted signals such as those due to antenna coupling and skin reflection. The tumour response will appear at different times in each of the two measurements, further enabling tumour localisation. The calibrated signals were afterwards transformed into time domain and fed into our UWB image reconstruction unit based on enhanced delay-and-sum algorithm [31].

3.1 Breast phantom with one tumour

In the first measurement, the breast phantom with one tumour of 1.3 cm diameter and at a depth of ~2 cm (off-centre) was placed inside the measurement system of Fig. 5. The calibrated signals

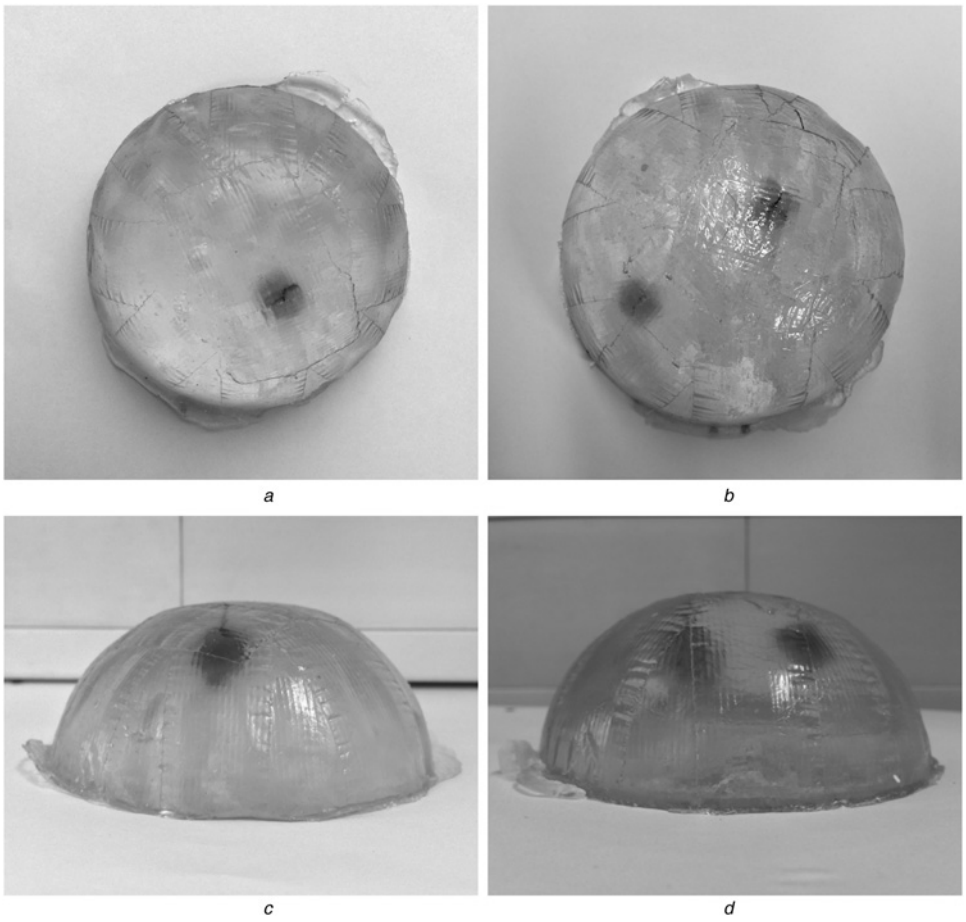

Fig. 7 *Synthesised breast phantoms of tumours, left and right columns*

a, c One tumour
b, d Two tumours

were processed in the reconstruction unit and in Fig. 8 the corresponding imaging results are displayed [all the imaging results present the two-dimensional (2D) slices of the relative energy map of the output of the beamformer]. Compared with the pictures of the phantom in Figs. 7*a* and *c*, it was observed that the tumour was successfully detected in the 3D space at the correct position in both $x-y$ and $x-z$ planes, however, with a different resolution. This was already expected, since the effective size of the array in the two views was different, thus leading to a different resolution.

3.2 Breast phantom with two tumours

For the second evaluation of the proposed measurement system, the phantom of Figs. 7*b* and *d* with two embedded tumours of different size and at different depths was used. One of the tumours had a diameter of ~1 cm and was located at a depth of 1.8 cm. The second tumour was 1.5 cm in diameter and 3 cm deep inside the breast phantom.

The image in Fig. 9 corresponds to the stacked $x-y$ plane image when looking at the phantom from above (i.e. all the images in the z-direction are added together). In this image, it is possible to recognise the two tumours: one approximately in the centre and the other nearly 4.5 cm above it. The reconstructed positions agree quite well with the real positions of the tumours.

To detect the depth of each tumour, we looked at the reconstructed images at different z (horizontal) layers. In Figs. 10 and 11, the images of six vertical planes are shown. The first three sub-figures corresponding to $z = 0.1$–2 cm show the first tumour near the centre ($z = 0$ points to the base of the phantom). The other three sub-figures, $z = 3$–5 cm, mainly include the second tumour that was located near the surface of the phantom. In Fig. 11*c* referring to the image of the phantom near the breast–air interface in the uppermost layer, a relatively large artefact is present that was due to the large reflections at the interface. Some quantitative results regarding the performance of the system are reported in Table 1. By comparing the actual position and depth of the tumours with the detected ones, it can be concluded that all the tumours were successfully detected in 3D space.

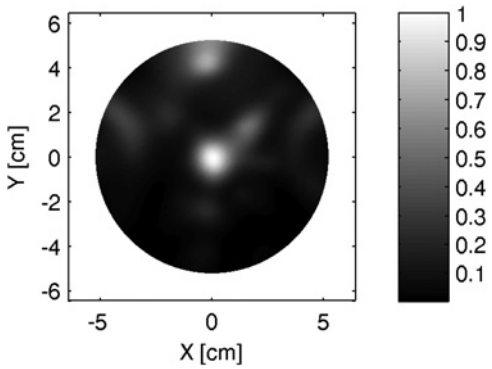

Fig. 9 *Stacked image of the breast phantom with two tumours in horizontal plane ($x-y$)*

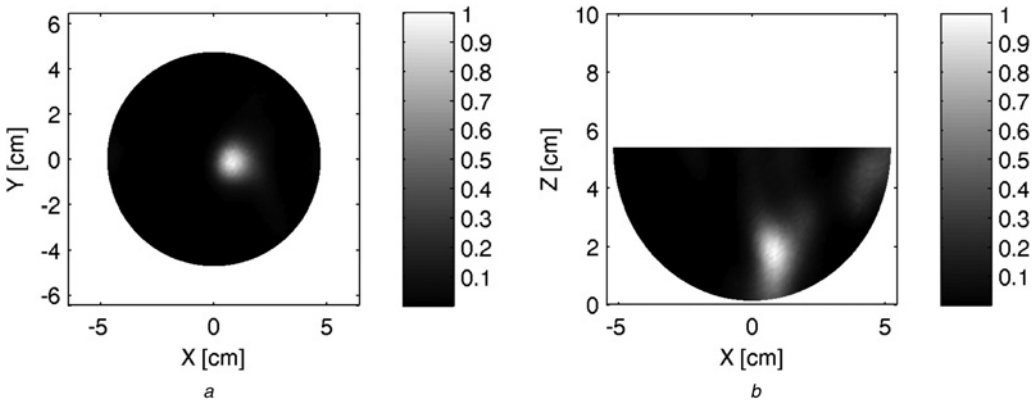

Fig. 8 *Imaging results of the one-tumour breast phantom in*

a Horizontal ($x-y$) plane
b Vertical ($x-z$) plane (linear scale)

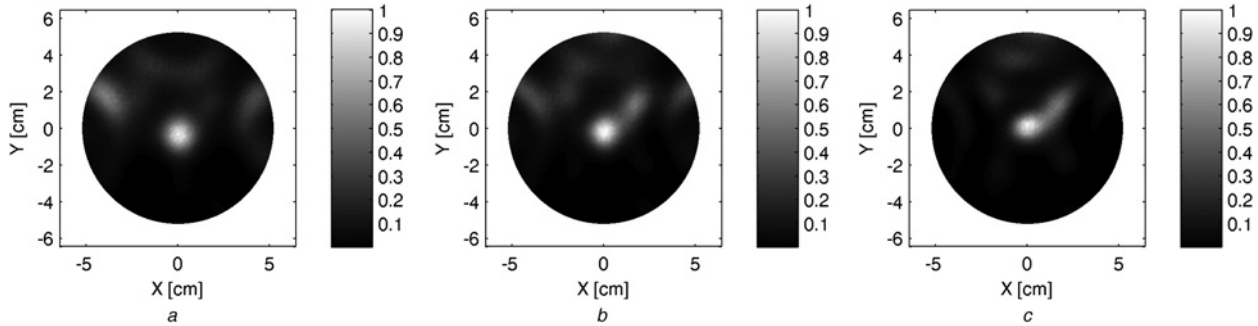

Fig. 10 *Imaging results corresponding to the two-tumour breast phantom at different horizontal layers (z-axis)*

a $z = 0.1$ cm
b $z = 1$ cm
c $z = 2$ cm

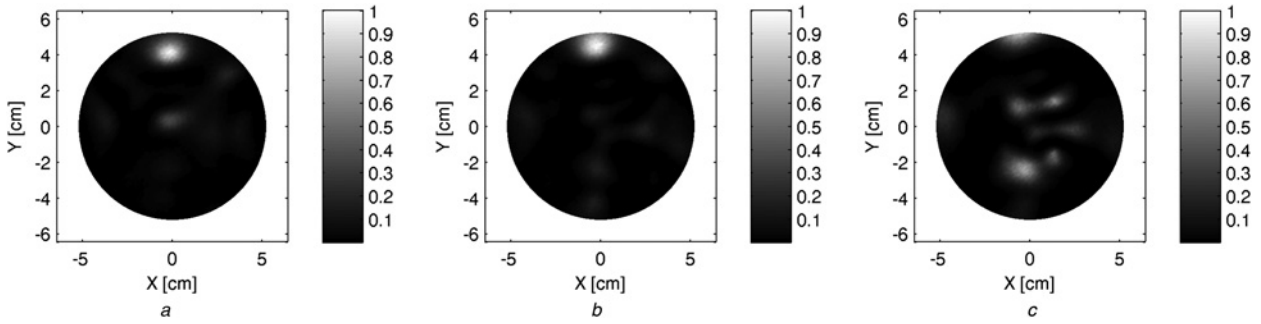

Fig. 11 *Imaging results corresponding to the two-tumour breast phantom at different horizontal layers (z-axis)*

a $z = 3$ cm
b $z = 4$ cm
c $z = 5$ cm

Table 1 Signal to clutter ratio (SCR) and position of tumours

Breast phantom	SCR, dB	Actual tumour position in cm (*x*, *y*, *z*)	Detected tumour position in cm (*x*, *y*, *z*)
with one tumour	4	(1.2, −1, 2)	(1, −0.1, 1.8)
with two tumours – tumour no. I	4.7	(0.6, 3.4, 1.8)	(−0.2, 4, 2)
with two tumours – tumour no. II	3.5	(0.8, −1, 3)	(0, −0.2, 3)

4 Conclusion

The design of a compact antenna element with large fractional bandwidth covering both low and high frequencies to ensure good penetration as well as high resolution is a challenge in microwave medical imaging. In this paper, an efficient compact bowtie antenna with the largest dimension of 15 mm and a bandwidth of 1.2 – 7 GHz was proposed for UWB near-field medical imaging and it was characterised via both simulations and measurements. The antenna was used inside a hemispherical array of 16 elements for the detection of breast cancer. The implemented near-field imaging system was evaluated using two average-tissue breast phantoms with one and two embedded tumours. The implemented imaging system was shown to operate efficiently in the presence of multiple tumours inside the breast phantom and it was able to detect the tumours. The successful detection of the tumours in both horizontal and vertical planes proved the efficiency and potential of the proposed UWB imaging system for breast cancer detection.

5 References

1 Hassan, A., El-shenawee, M.: 'Review of electromagnetic techniques for breast cancer detection', *IEEE Rev. Biomed. Eng.*, 2011, **4**, pp. 103–118
2 Fear, E., Meaney, P., Stuchly, M.: 'Microwaves for breast cancer detection?', *IEEE Potentials*, 2003, **22**, (1), pp. 12–18
3 Shahzad, A., O'Halloran, M., Jones, E., Glavin, M.: 'Prefiltered beamforming for early-stage breast cancer detection', *IEEE Antennas Wirel. Propag. Lett.*, 2013, **12**, pp. 500–503
4 Klemm, M., Craddock, I.J., Leendertz, J.A., Preece, A., Benjamin, R.: 'Improved delay-and-sum beamforming algorithm for breast cancer detection', *Int. J. Antennas Propag.*, 2008, **2008**, pp. 1–9
5 O'Halloran, M., Glavin, M., Jones, E.: 'Quasi-multistatic MIST beamforming for the early detection of breast cancer', *IEEE Trans. Biomed. Eng.*, 2010, **57**, (4), pp. 830–840
6 Lim, H.B., Nhung, N.T.T., Li, E.-P., Thang, N.D.: 'Confocal microwave imaging for breast cancer detection: delay-multiply-and-sum image reconstruction algorithm', *IEEE Trans. Biomed. Eng.*, 2008, **55**, (6), pp. 1697–1704
7 Porter, E., Kirshin, E., Santorelli, A., Coates, M., Popović, M.: 'Time-domain multistatic radar system for microwave breast screening', *IEEE Antennas Wirel. Propag. Lett.*, 2013, **12**, pp. 229–232
8 Golnabi, A.H., Meaney, P.M., Paulsen, K.D.: 'Tomographic microwave imaging with incorporated prior spatial information', *IEEE Trans. Microw. Tech.*, 2013, **61**, (5), pp. 2129–2136
9 Golnabi, A.H., Meaney, P.M., Geimer, S., Zhou, T., Paulsen, K.D.: 'Microwave tomography for bone imaging'. Proc. of IEEE Int. Symp. on Biomedical Imaging: From Nano to Macro, Chicago, IL, 2011, pp. 956–959
10 Persson, M., Fhager, A., Dobsıcek Trefna, H., *et al.*: 'Microwave-based stroke diagnosis making global prehospital thrombolytic treatment possible', *IEEE Trans. Biomed. Eng.*, 2014, **61**, (11), pp. 2806–2817
11 Sharyl, I.C.H., Nass, J., Lashof, J.C.: 'Mammography and beyond: developing technologies for the early detection of breast cancer' (National Academies Press, Washington, USA, 2001)
12 Lazebnik, M., Popovic, D., McCartney, L., *et al.*: 'A large-scale study of the ultrawideband microwave dielectric properties of normal, benign and malignant breast tissues obtained from cancer surgeries', *Phys. Med. Biol.*, 2007, **52**, pp. 6093–6115
13 Henriksson, T., Klemm, M., Gibbins, D., *et al.*: 'Clinical trials of a multistatic UWB radar for breast imaging'. Proc. of Antennas and Propagation Conf. (LAPC), Loughborough, 2011, pp. 1–4
14 Klemm, M., Gibbins, D., Leendertz, J., *et al.*: 'Development and testing of a 60-element UWB conformal array for breast cancer imaging'. Proc. of Antennas Propagation (EUCAP), Rome, 2011, pp. 3377–3379
15 Schwarz, U., Thiel, F., Seifert, F., Stephan, R., Hein, M.A.: 'Ultrawideband antennas for magnetic resonance imaging navigator techniques', *IEEE Trans. Antennas Propag.*, 2010, **58**, (6), pp. 2107–2112
16 Wang, X., Bauer, D.R., Witte, R., Xin, H.: 'Microwave-induced thermoacoustic imaging model for potential breast cancer detection', *IEEE Trans. Biomed. Eng.*, 2012, **59**, (10), pp. 2782–2791
17 Eskandari, A.R., Naser-Moghaddasi, M., Virdee, B.S.: 'Target identification enhancement using a combination of linear sampling method and adjoint sensitivity analysis', *IET Microw. Antennas Propag.*, 2012, **6**, (4), pp. 461–469
18 Brignone, M., Coyle, J., Piana, M.: 'The use of the linear sampling method for obtaining super-resolution effects in Born approximation', *J. Comput. Appl. Math.*, 2007, **203**, pp. 145–158
19 Joachimowicz, N., Pichot, C., Hugonin, J.P.: 'Inverse scattering: an iterative numerical method for electromagnetic imaging', *IEEE Trans. Antennas Propag.*, 1991, **39**, (12), pp. 1742–1753
20 Grzegorczyk, T., Meaney, P., Kaufman, P., di Florio-Alexander, R., Paulsen, K.: 'Fast 3-D tomographic microwave imaging for breast cancer detection', *IEEE Trans. Med. Imaging*, 2012, **31**, (8), pp. 1584–1592
21 Nilavalan, R., Craddock, I.J., Preece, A., Leendertz, J., Benjamin, R.: 'Wideband microstrip patch antenna design for breast cancer tumour detection', *IET Microw. Antennas Propag.*, 2007, **1**, (2), pp. 277–281
22 Gibbins, D., Klemm, M., Craddock, I.J., Leendertz, J.A., Preece, A., Benjamin, R.: 'A comparison of a wide-slot and a stacked patch antenna for the purpose of breast cancer detection', *IEEE Trans. Antennas Propag.*, 2010, **58**, (3), pp. 665–674
23 Bassi, M., Caruso, M., Saeed Khan, M., Bevilacqua, A., Capobianco, A.D., Neviani, A.: 'An integrated microwave imaging radar with planar antennas for breast cancer detection', *IEEE Trans. Microw. Tech.*, 2013, **61**, (5), pp. 2108–2118
24 Sugitani, T., Kubota, S., Toya, A., Xiao, X., Kikkawa, T.: 'A compact 4 at × 4 planar UWB antenna array for 3-D breast cancer detection', *IEEE Antennas Wirel. Propag. Lett.*, 2013, **12**, pp. 733–736
25 See, C.H., Abd-Alhameed, R.A., Chung, S.W.J., Zhou, D., Al-Ahmad, H., Excell, P.S.: 'The design of a resistively loaded bowtie antenna for applications in breast cancer detection systems', *IEEE Trans. Antennas Propag.*, 2012, **60**, (5), pp. 2526–2530
26 Jalilvand, M., Li, X., Kowalewski, J., Zwick, T.: 'Broadband miniaturized bowtie antenna for 3D microwave tomography', *IET Electron. Lett.*, 2014, **50**, (4), pp. 244–246
27 Li, X., Jalilvand, M., Sit, L., Zwick, T.: 'A Compact double-layer on-body matched bowtie antenna for medical diagnostics', *IEEE Trans. Antennas Propag.*, 2014, **62**, (4), pp. 1808–1816
28 Li, X., Jalilvand, M., Zwirello, L., Zwick, T.: 'Array configurations of a UWB near field imaging system for the detection of water accumulation in human body'. Proc. of European Radar Conf. (EuRAD), Rome, Italy, 2011, pp. 170–173
29 Gabriel, S., Lau, R.W., Gabriel, C.: 'The dielectric properties of biological tissues: III. Parametric models for the dielectric spectrum of tissues', *Phys. Med. Biol.*, 1996, **41**, pp. 2271–2293
30 Klemm, M., Craddock, I.J., Leendertz, J.A., Preece, A., Benjamin, R.: 'Radar-based breast cancer detection using a hemispherical antenna array – experimental results', *IEEE Trans. Antennas Propag.*, 2009, **57**, (6), pp. 1692–1704
31 Jalilvand, M., Pancera, E., Li, X., Zwick, T., Wiesbeck, W.: 'A sparse synthetic aperture-based UWB medical imaging system'. Proc. of Microwave Conf. (GeMIC), Darmstadt, Germany, 2011, pp. 1–4